remote sensing

MDPI

Article

Integrated Approaches for Field Mapping by Traditional Investigation and Satellite PSInSAR Data: Results from the Montemartano Landslide (Central Italy)

Lucio Di Matteo [1,*], Riccardo Cardinali [2], Valentina Cerboni [1], Fabio Guadagnano [1], Giorgio Piagnani [3], Claudia Ribaldi [4], Biagio Marco Sotera [5] and Corrado Cencetti [1]

[1] Dipartimento di Fisica e Geologia, Università degli Studi di Perugia, 06123 Perugia, Italy
[2] Comune di Spoleto, 06049 Spoleto, Italy
[3] Geoland, 06083 Bastia Umbra, Italy
[4] Geoter Ambiente, 06123 Perugia, Italy
[5] Independent Researcher, 06049 Spoleto, Italy
* Correspondence: lucio.dimatteo@unipg.it; Tel.: +39-0755849694

Abstract: The study presents an integrated investigation of a complex landslide based on multitemporal stereo aerial photographic interpretations, existing geotechnical monitoring data, and different PSInSAR datasets. The available information allowed for the quantification of the deformation history, also in periods with no monitoring in the field, making it possible to revise the geometry of the landslide compared to the official landslide mapping. Data from sparse inclinometers are compared with more spatially continuous satellite measurements, showing that the two monitoring techniques are consistent in terms of cumulative deformation trend and in terms of response to prolonged drought and wet periods. Therefore, reliable landslide mass displacements can be monitored using satellite products when ground instrumentations are no longer operating. Understanding the landslide behavior to rainfall conditions offers an important insight into the velocities and cumulative displacements expected during similar stages of enhanced landslide activity. The findings can be helpful to support urban planners in re-evaluating hazard and risk classification and implementing efficient mitigation techniques to reduce landslide damage.

Keywords: PSInSAR; ERS; ENVISAT; COSMO-SkyMed; complex landslide; ground-based monitoring; landslide mapping

Citation: Di Matteo, L.; Cardinali, R.; Cerboni, V.; Guadagnano, F.; Piagnani, G.; Ribaldi, C.; Sotera, B.M.; Cencetti, C. Integrated Approaches for Field Mapping by Traditional Investigation and Satellite PSInSAR Data: Results from the Montemartano Landslide (Central Italy). *Remote Sens.* **2023**, *15*, 1221. https://doi.org/10.3390/rs15051221

Academic Editors: Lisa Borgatti, Enrico Borgogno-Mondino, Alessandro Corsini, Daniele Giordan, Stefano Gandolfi and Mauro Soldati

Received: 30 January 2023
Revised: 16 February 2023
Accepted: 20 February 2023
Published: 22 February 2023

1. Introduction

Landslide mapping is the key element of assessing landslide risk and the primary step for landslide prevention [1]. Field surveys, including geomorphological, geotechnical, and geophysical investigations, can provide detailed data for a landslide study, useful for obtaining information about the shape and movement of a landslide [2–4]. Although these approaches are commonly used in the recognition and study of landslides, they can be time-consuming and, in some cases (e.g., large landslide areas, where the topography is hummocky and/or the vegetation is dense, etc.) could be inefficient in identifying all the parts of a landslide [5]. Moreover, it can be difficult to follow a landslide boundary in the field because it is often indistinct [6]. During the past decades, studies have paid attention to approaches for site-specific landslide mapping and analysis based on the integration of traditional field surveys and remote sensing investigations, including GPS monitoring, e.g., [7], multitemporal satellite Synthetic Aperture Radar Interferometry (InSAR) and Ground-Based InSAR monitoring [8–17]. The measure and monitoring of targets without a direct approach to the landslide source area is increasingly used, making satellite PSInSAR (Permanent Scatterers InSAR) investigations an effective tool to investigate the deformations induced by relatively rapid landslides, contributing to more accurate and

complete landslide mapping. This approach can also help revise the Landslide Inventory Maps (LIMs) and assess landslide hazards and risks. The need for updated knowledge on landslides is a very timely issue; according to the River Basin District Authorities (RBDA), the 10% territory of Central Italy is interested by high and very-high landslide hazard areas (P3 and P4) on a scale from P1 to P4 [18]. The existing landslide mapping was obtained by multitemporal aerial photographic interpretations coupled—in a few cases—with information taken by field surveys. Since the landslide mapping of the RBDA planning is a dynamic instrument, it may be subject to change over time following new studies and surveys [18]. The 2016 earthquake in Central Italy (mainshocks up to Mw 6.5) produced several co-seismic effects [19–25], including the triggering of hundreds of landslides [26–31], which requires the implementation of the existing landslide inventory.

Currently, a re-assessment of hazard and risk affecting landslide areas is taking place in the territory managed by the Autorità di Bacino Distrettuale dell'Appennino Centrale (ABDAC) by integrating updated field data and multitemporal satellite PSInSAR investigations, which allows measuring ground displacements occurring during a defined range of time with millimeter accuracy [32]. In the framework of an agreement with ABDAC, the University of Perugia is carrying out the revision of about 100 landslides falling in 12 municipalities of the Umbria Region affected by the earthquakes in Central Italy in 2016 (https://www.modom.it/elenco-comuni-terremoto-2016, accessed on 9 January 2023). Among the landslides examined, the Montemartano landslide (Spoleto, Central Italy) is taken as reference, a complex landslide (rotational slide-earth flows) involving debris and clayey layers lying on highly tectonized calcareous and marly-arenaceous bedrock. According to Grana e Tommasi [33], even though the slope processes are slow for this type of landslide, it frequently affects dwellings and roads connecting villages situated on the stable parts of the mountain flanks. The main objective of the research is to improve the Montemartano landslide map by integrating results from new geomorphological surveys, multitemporal aerial photographic interpretations, existing geotechnical monitoring data, and satellite remote-sensing PSInSAR technique. Different satellite systems are considered, such as ERS 1–2 and ENVISAT archives (operating in the microwave C-band) and COSMO-SkyMed, CSK (operating in the X-band). Moreover, the assessment of hazard and risk is presented providing information for the land-use planning to the local and administrative authorities in charge of landslide hazard management.

2. Study Area

2.1. Geological and Geomorphological Setting

The Montemartano landslide is located in the eastern part of the Monti Martani ridge (Figure 1), a box-shaped anticline oriented NW–SE involving the deformation of the sedimentary rocks of the Umbria–Marche sequence. An overthrust, dipping towards WSW–SSW, determines the overlapping of the series on an eastward syncline [34].

The landslide area is included in the central sector of the anticline, where the structure takes an NNW–SSE direction and is overturned with a series of minor folds involving marly–clayey rocks. The area is characterized by the outcropping of the Umbria–Marche sequence from the Scaglia Rossa, SAA (stratified and fractured pelagic limestones and marly limestones, Turonian–middle Eocene) to Bisciaro, BIS (ochraceous marls and marly limestones, Aquitanian–Burdigalian), and Schlier, SCH (grey silty–clayey marls, Burdigalian). Figure 1 shows the geological map of the study area as derived from the digital geological mapping for GIS systems by the Umbria Region (https://dati.regione.umbria.it/dataset/carta-geologica-dell-umbria, accessed on 9 January 2023). Debris deposits, remolded clayey layers, and part of the disarticulated rock layers of the Bisciaro formation characterize the landslide mass. The bedrock is mainly composed of the Bisciaro and Schlier formations, the upper part of which is softened and fractured due to the minor folds developing in a compressive stress environment (see the geological section in Figure 1). The historic center of the Montemartano village (altitude of 570 m a.s.l.) is located on the Bisciaro formation that is lowered by a NE–SW normal fault.

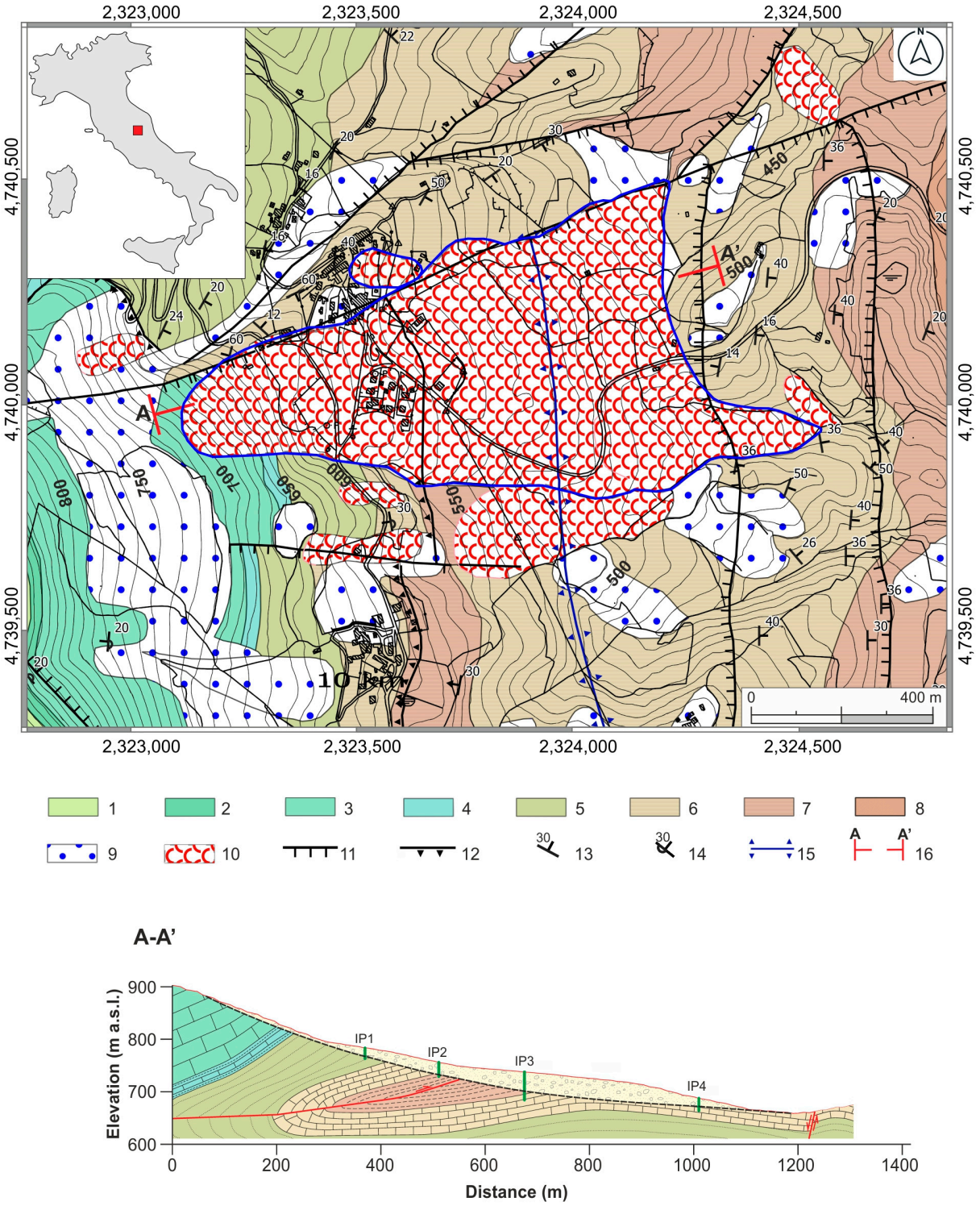

Figure 1. Geological map of the Montemartano landslide area, based on the geopackage of Umbria Region (https://www.onegis.it/2019/06/19/cartografia-geologica-umbria-stilizzata-per-qgis/, accessed on 10 January 2023), with an NE–SW geological cross section. (1) Marne a Fucoidi–FUC; (2) Scaglia Bianca–SBI; (3) Scaglia Rossa–SAA; (4) Scaglia Variegata–VAS; (5) Scaglia Cinerea–SCC; (6) Bisciaro–BIS; (7) Schlier–SCH; (8) Marnoso-Arenacea Romagnola (Galatea member)–FMA; (9) Talus; (10) Landslides; (11) Normal fault; (12) Thrust; (13) Dip direction of beds; (14) Inverted beds; (15) Anticlinal axis; (16) Geological cross-section trace.

From a geomorphological perspective, the area can be divided into two zones that exhibit distinct characteristics: a mountainous western part (slope angle of 20–30°) and a hilly-type eastern part (slope angle of about 15°). The latter includes most parts of the landslide area, which shows widespread surface deformations, flattened areas, and terraces responsible for several damage to buildings and infrastructure. Figure 2 shows the main geomorphological features in the different landslide parts, with some examples of cracks, distortions and dislocations produced by mass movements on some structures.

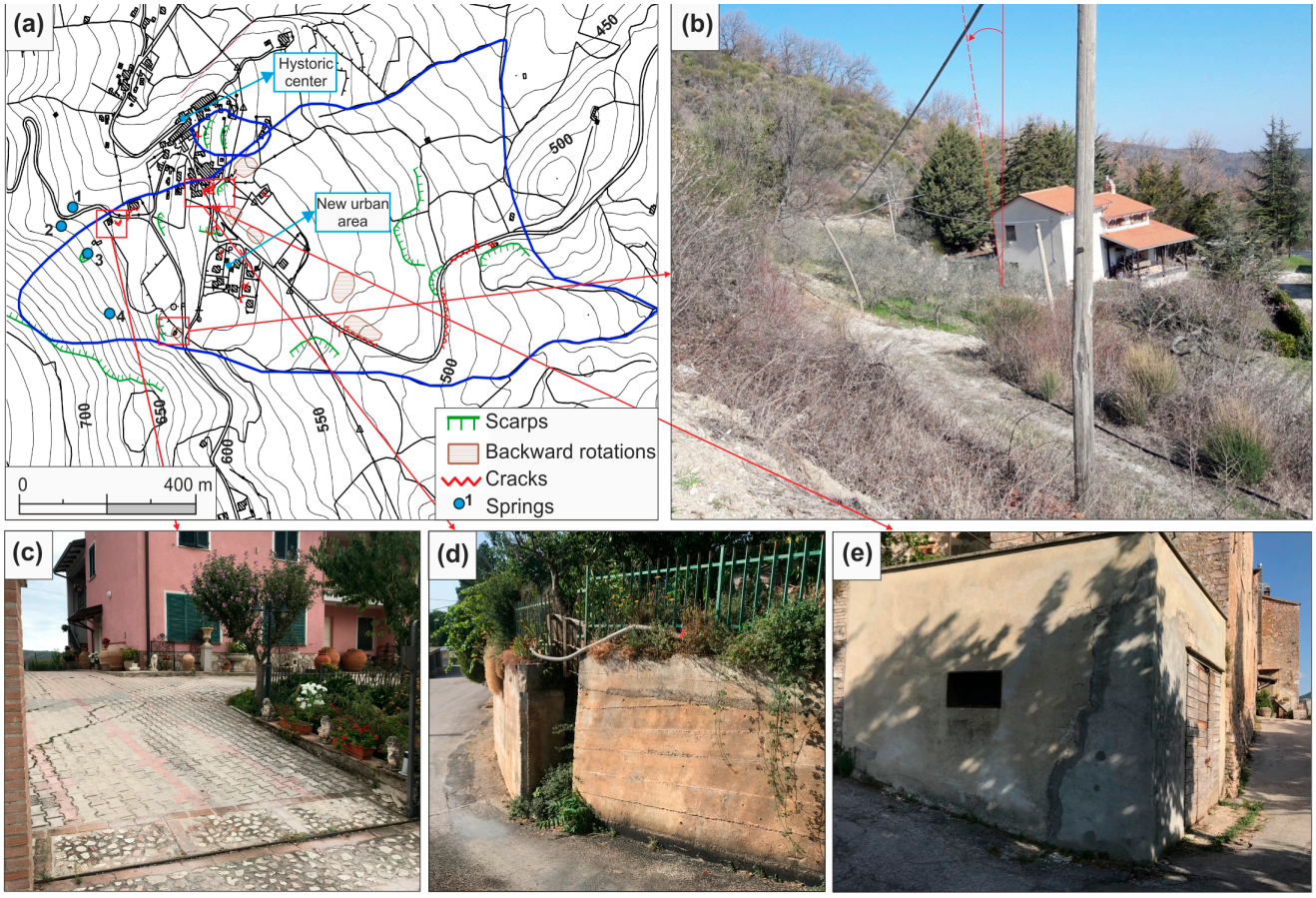

Figure 2. (**a**) Main geomorphological features obtained by the field survey with some examples of effects produced by the landslide on some structures; (**b**) Backward rotation of a sparse house; (**c**) Cracks in the floor pertaining to a dwelling; (**d**) Opening of a retaining wall; (**e**) Cracking on a building wall.

In the landslide head scarp area, some springs are fed by groundwater hosted in the Scaglia Rossa formation, emerging at contact with the low-permeability Scaglia Variegata formation. A detailed survey along the head scarp area showed that the draining system of springs is founded on the debris outcropping along the slope. As Alta Scuola [35] reported, the draining system of spring n. 3 in Figure 2 has been progressively detached due to the movement of that debris body. Despite extensive remedial work in the late 1990s, in 2004, the drainage tunnel showed new signs of movement. This information gave valuable insights into the delimitation of the extent of the landslide perimeter in the head scarp area, which included the debris body responsible for the movement of the drainage tunnels of the springs.

3. Materials and Methods

3.1. Characteristic of Landslide Mass Materials and Field Monitoring Data

The Montemartano landslide area was surveyed for the first time in 2002 to characterize the landslide materials overlying the bedrock and implement a monitoring plan between 2003 and 2005, with new data acquired in 2008. The pioneer studies were carried out by Grana and Tommasi [33] and Alta Scuola [35], who reported and analyzed the results of the geognostic surveys (2002 campaign), and the monitoring campaign carried out during 2003–2005. The monitoring system was integrated in 2008 (IP3) with new information collected in 2018–2019 by Regione Umbria [36]. Table 1 shows a synthesis of instruments, geotechnical and geophysical investigations within the landslide area taken from the above studies.

Table 1. Synthesis of instruments, geotechnical and geophysical investigations within the landslide area. I = inclinometer; P = Piezometer; DPSH = Dynamic Probing Super Heavy test.

Name	Type	Depth (m)	Monitoring Period or Test Execution Date
IP2	Borehole with I and P	27.3	n. 3 acquisition during October 2003–April 2004
IP3	Borehole with I and P	54.5	n. 4 acquisition during January 2008–December 2008
IP4	Borehole with I and P	23.5	n. 8 acquisition during February 2003–May 2004
IP5	Borehole with I and P	15.0	n. 8 acquisition during February 2003–April 2004
IP6	Borehole with I and P	23.0	n. 14 acquisition during February 2003–March 2005
IP8	Borehole with I and P	21.0	n. 8 acquisition during March 2003–May 2004
IP9	Borehole with I and P	18.0	n. 6 acquisition during February 2003–February 2004
IP11	Borehole with I and P	12.0	n. 8 acquisition during February 2003–July 2004
IP20	Borehole with I and P	17.0	n. 8 acquisition during April 2003–June 2004
IP21	Borehole with I and P	34.0	n. 1 acquisition in 2018
P1	DPSH	4.0	7 October 2002
P2	DPSH	11.0	7 October 2002
P3	DPSH	7.0	7 October 2002
P4	DPSH	6.0	7 October 2002
P5	DPSH	9.2	7 October 2002
P6	DPSH	8.8	8 October 2002
P7	DPSH	10.6	8 October 2002
P9	DPSH	9.0	15 October 2002
P10	DPSH	9.4	15 October 2002
P11	DPSH	4.6	15 October 2002
P12	DPSH	6.2	8 October 2002
P13	DPSH	5.2	15 October 2002
P14	DPSH	13.8	15 October 2002
P15	DPSH	7.8	16 October 2002
P16	DPSH	12.2	15 October 2002
CH1	Cross-hole	50.0	October 2002
CH2	Cross-hole	50.0	October 2002
CH3	Cross-hole	50.0	October 2002

Figure 3 shows the location of the field geotechnical investigations and the monitoring system, including a rain gauge (Montemartano, 618 m a.s.l., coordinates WGS84

12.5947222–42.7880555) installed in 2008 in the crown zone of the landslide, which helps investigating the effect of prolonged rainfall periods on the landslide movement. Before 2008, rainfall data were available from the San Silvestro rain gauge (383 m a.s.l., coordinates WGS84 12.6738888–42.7558333), located about 5 km SE of Montemartano. Standard Penetration Tests in boreholes (SPT) and Dynamic Probing Super Heavy tests (DPSH) were used to distinguish the transition between remolded materials and more preserved soil structures in the landslide mass [36]. These tests were integrated with the results of the cross-hole seismic profiles; the shear waves velocity (V_S) in CH2 (Figure 3) reached a maximum value of about 1600 m/s seismic at the top of the bedrock (16–19 m depth) with values lower than 1200 m/s in the overlying layers.

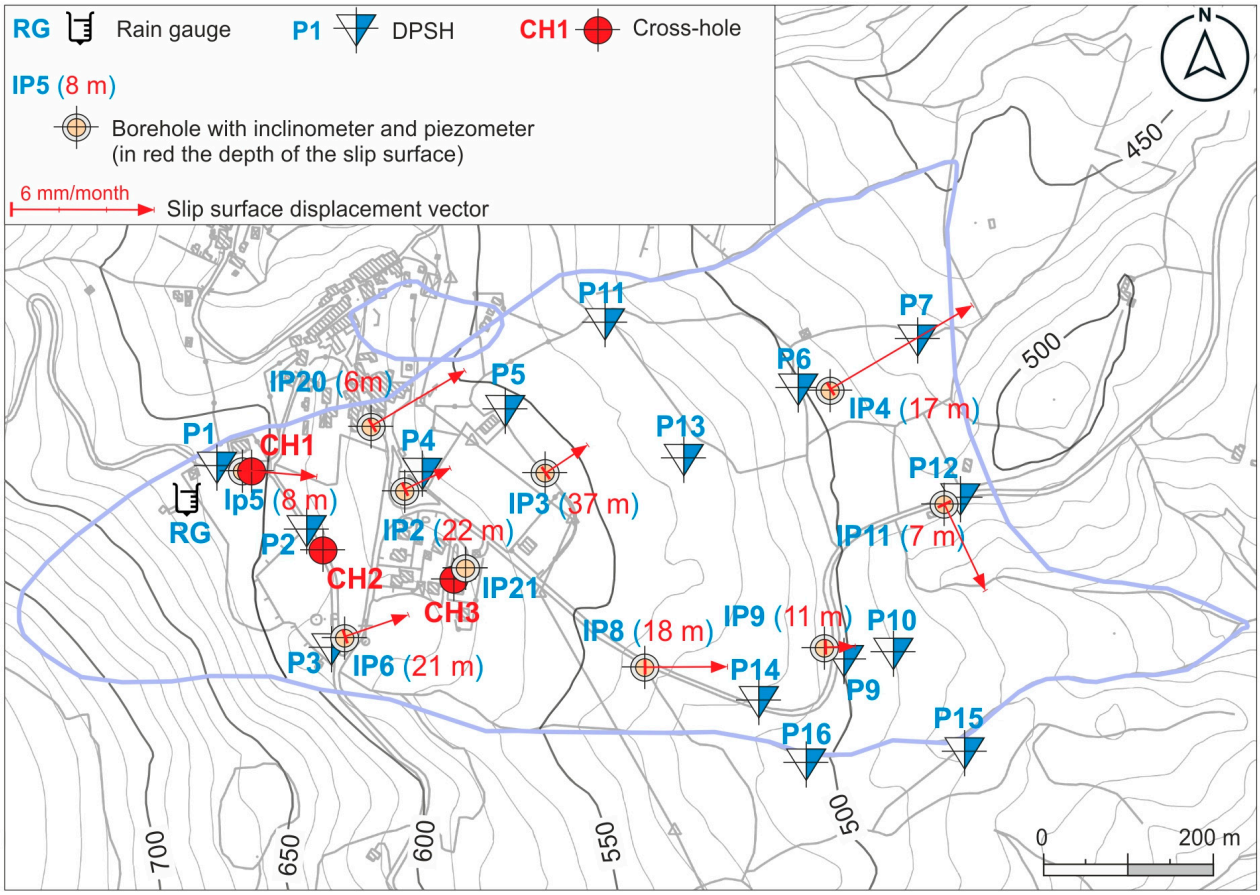

Figure 3. Location of the rain gauge, field investigations, and landslide mass monitoring system (only those falling in the landslide area are reported). Displacement vectors (maximum values during the monitoring period) and the depth of the slip surface were obtained with data collected during the monitoring campaign carried out between February 2003–May 2004, except for IP3, the data of which are referred to 2008.

Materials are mainly characterized by low- to medium-plasticity soils with Plasticity Index (PI) in the range 8–20% and low Clay Fraction (CF = 8–15%). Moreover, the residual shear strength angle values (φ'_R) along pre-existing surfaces show a bimodal distribution with the most recurrent values of 13° and 22° [33,35].

Inclinometers were installed in ten boreholes with monthly measurements carried out between February 2003–May 2004, representing the only monitoring campaign investigating most of the landslide area. An additional inclinometer was installed in 2008 (IP3 in Figure 3), and a new monitoring campaign, highlighting no significant displacements, was carried out on IP21 in 2018–2019. Unfortunately, as reported by [36], the latest monitoring campaign (2018–2019) highlighted that all the inclinometers placed in the past, excluding

IP21, were damaged by the landslide movements, making them ineffective. By analyzing the data of the different monitoring campaigns, the maximum depth of the slip surface was registered at about 38 m (IP3, Figure 3). The maximum displacement vector was recorded during 2004 (6.6 mm/month in IP8 inclinometer, Figure 3).

3.2. Historical Aerial Photographs

Photo interpretation is one of the simplest but fundamental techniques for identifying landslides. It consists of an integrated study of several indicators, such as photographic (tone, texture, pattern), morphological (shapes, slopes, concavity, and convexity, etc.) and photogeological (lithology, stratification, and discontinuity surfaces). In particular, the multi-temporal photo interpretation of the same landslide area represents a valuable tool to assess the different morphological evolutionary phases due to natural and anthropic processes [37–39]. In the case of the Montemartano landslide, an extensive repository of aerophotographic materials from the Umbria Region is available. The flights cover about 40 years, from the post-war period to the end of the 20th century, in which the anthropogenic component of the landscape, linked to increasing urban and infrastructural development and transformations of agricultural activities, often prevailed over the natural one. Photointerpretation was carried out using specific software (Menci Z-Map Photo, version 3.6) on a PC workstation with a suitable graphics card and monitor 3d capable of managing high-resolution frames in a digital format derived from aerial photo scans. A free image editor (StereoPhoto Maker-https://stereo.jpn.org/eng/stphmkr/, accessed on 10 January 2023) made it possible to create stereographic images (anaglyphs), which can be observed by the operator equipped with bicolor or polarized glasses. Table 2 shows the information about the frames used for the multi-temporal comparison of the landslide area.

Table 2. Characteristics of the imagery database used in the study area.

Type	Date	Scale	Executing Company	Flight Strips	Photograms
AR 06–"Volo GAI" B/W	1954–55	1:33.000	Istituto Geografico Militare	32 33	733–734–735 929–930
"Volo Umbria a colori"	1977	1:13.000	Compagnia Generale Riprese Aeree di Parma	43A	049–050
"Volo AR34" B/W	1996–1997	1:28.000	Compagnia Generale Riprese Aeree di Parma	2	4019–4020

3.3. PSInSAR Technique

The PSInSAR is a technique for processing satellite data that allows the estimation of displacements of the Earth's surface, proving efficient in the monitoring of low deformation phenomena belonging to "extremely-slow" to "very-slow" classes according to [40]. It is based on using a time series of SAR satellite images [41,42]. A radar sensor mounted on the satellite radiates an electromagnetic pulse towards stable reflectors, both natural and anthropic, located on the Earth's surface, which reflects the backscattered signal [43]. By measuring the time elapsed between sending the signal and receiving the backscattered component, the radar system can determine, with millimeter accuracy, the distance between the sensor and the target [13,32].

According to Pigorini et al. [44], SAR datasets covering the Italian territory are available from 1992 (ERS 1–2 satellite), followed by other SAR sensors orbiting the Earth, such as ENVISAT and CSK. Table 3 shows the main characteristics and resolution of the different datasets for PSInSAR analysis in the Montemartano landslide area.

Table 3. Characteristics of the satellite images.

Satellite	Property	Revising Time (Days)	Resolution (Azimuth × Range)	Band	Period
ERS 1–2	European Space Agency (ESA)	35	20 × 5 m	C	1992–2000
ENVISAT	European Space Agency (ESA)	35	20 × 5 m	C	2003–2010
Cosmo SkyMed (CSK)	Italian Space Agency (ASI)	8	up to 1 × 1 m	X	2011–2014

The PS outputs include the average displacement rates over the observed period and the time series of the deformation per point, providing information on the temporal evolution of the displacements [13]. According to Ciampalini et al. [45], satellite sensors are side-looking and can acquire images in two different geometries, ascending (following an approximately S–N direction) and descending (following an approximately N–S direction). In detail, observations with the ascending geometry are suitable for detecting movements on west-facing slopes. In contrast, the descending geometry ones are suitable for detecting movements located on east-facing slopes. The analysis of PS time series allows for studying the evolution of displacements in the different seasons, also considering the meteo-climatic conditions. For each target, cumulated displacement values (mm), the annual rate of deformation (mm/year) and the quality parameters (standard deviation, stdev., and coherence, coher.) are reported. The displacement of PS is represented by a color scale gradation from red (negative values) to blue (positive values).

3.4. Hazard and Risk Assessment Method

The hazard and risk assessment procedure in the territories currently managed by ABDAC (about 42.500 km^2) has been developed as part of the Piano Stralcio di Assetto Idrogeologico del F. Tevere (PAI) [46].

Four levels of hazard are defined: P1 (moderate); P2 (medium); P3 (high); P4 (very high), which correspond to possible actions that can be performed on the territory. In the case of P3, building enlargement for hygienic and sanitary adaptations is permitted. In P4 areas, vulnerability reduction actions can be implemented (no increase in the surface and volume of buildings). After defining the landslide through specific analyses (geomorphological survey, photo-interpretation, etc.), the procedure includes different steps, allowing a uniform assessment of the specific risk and the predicted total risk for different landslide types and different classes of exposed elements. Figure 4 shows the different steps to obtain the hazard and total risk for a sliding landslide characterized by slow movements, such as the Montemartano one.

Step 1 allows a preliminary definition of the intensity of the landslide based on the estimated volume, which ranges from 1 to 4 (from fair to very high). The intensity obtained in Step 1 is used in Step 2 to obtain the hazard by considering the frequency of the landslide occurrence over 50 years (e.g., from one event to more than three events in the selected period). As shown in Figure 4 the color of the cells indicates the hazard level.

Step 3 uses an expedition criterion for estimating the expected damage based on the relationships between the element at risk and the intensity and type of the expected landslide. For each element at risk (building, infrastructure, and population), a specific level of damage is assigned from 100 to 300. In general, the expected damage for landslide sliding types on buildings move from non-structural (100), in the case of fair intensity, to structural (300), in the case of very high intensity. Step 4 allows the definition of the specific risk based on the vulnerability and hazard resulting from the previous steps. In practice, each color of the cells in step 4 corresponds to the risk level described in step 5, from R1 to R4.

Step 1: evaluation of the landslide intesity

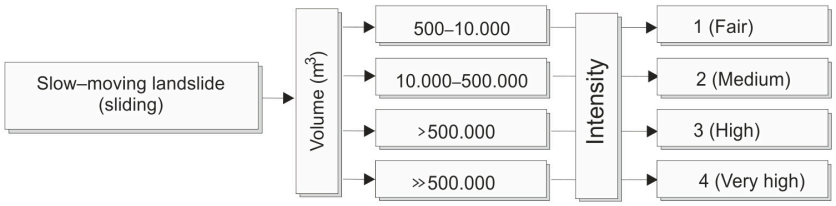

Step 2: evaluation of the landslide hazard

Frequency*	Intensity			
	1 (Fair)	2 (Medium)	3 (High)	4 (Very high)
10 (Low)	11	12	13	14
20 (Medium)	21	22	23	24
30 (High)	31	32	33	34
40 (Very high)	41	42	43	44

* based on n. of events in 50 years. Low = 1; Medium = 2; High = 3; Very high>3

Hazard levels: P1 P2 P3 P4

Step 3: Estimation of the expected damage for the identified risk elements (buildings, infrastructure, and population).

E = Non-structural damage (100); F = functional losses (200), S = structural damage (300).

Step 4: evaluation of the landslide specif risk based on hazard and vulnerability

Hazard	Vulnerability		
	100 Non-structural damage	200 Functional losses	300 Structural damage
11	111	211	311
12	112	212	312
13	113	213	313
21	121	221	321
14	114	214	314
22	122	222	322
23	123	223	323
31	131	231	331
32	132	232	332
24	124	224	324
33	133	233	333
41	141	241	341
42	142	242	342
34	134	234	334
43	143	243	343
44	144	244	344

Step 5: definition of the level of risk

Risk class	Risk level	Building and facilities	Population
R1	Moderate	Marginal socio–economic and environmental damage	No damage
R2	Medium	Aesthetic damage to buildings, aesthetic and functional damage to infrastructures and to the environmental heritage	No damage
R3	High	Functional and structural damage to buildings, infrastructures and environmental heritage	Homeless, indirect damage to socio–economic activities
R4	Very high	Functional and structural damage to buildings, infrastructures and environmental heritage	Fatalities, injured, homeless, damage to socio–economic activities

Figure 4. Landslide risk assessment procedure for the Tiber River Basin District Authority (Piano di Assetto Idrogeologico, PAI [46]).

4. Results

Integrating field surveys, multitemporal aerial photographic interpretations, existing geotechnical monitoring data, and satellite PSInSAR monitoring allow updating the Montemartano landslide map, highlighting parts of the landslide mass where movements are affecting infrastructure and housing.

The multitemporal stereoscopic analysis—based on the interpretation of the aerial photos listed in Table 2—indicates that in all three photo-interpreted flights, the area is affected by vast zones of active landslides characterized by complex movements with the combination of roto-translational sliding and flow mechanisms. The largest landslide area is south of the Montemartano village, characterized by a detachment area with high escarpments (set on the calcareous bedrock), which appeared in 1954 to be very eroded and devoid of vegetation, subsequently covered by dense forest cover (Figure 5a). Downslope, the morphology appears very articulated with successions of terraces. In the flights of 1977 and 1997 (Figure 5b,c), the presence of localized secondary movements within the vast landslide area does not alter its general planimetric configuration. Overall, landslide movements develop on layers of debris and ancient landslides, showing a frequent tendency to a coalescence of detachment niches and/or accumulations and occupy entire watersheds.

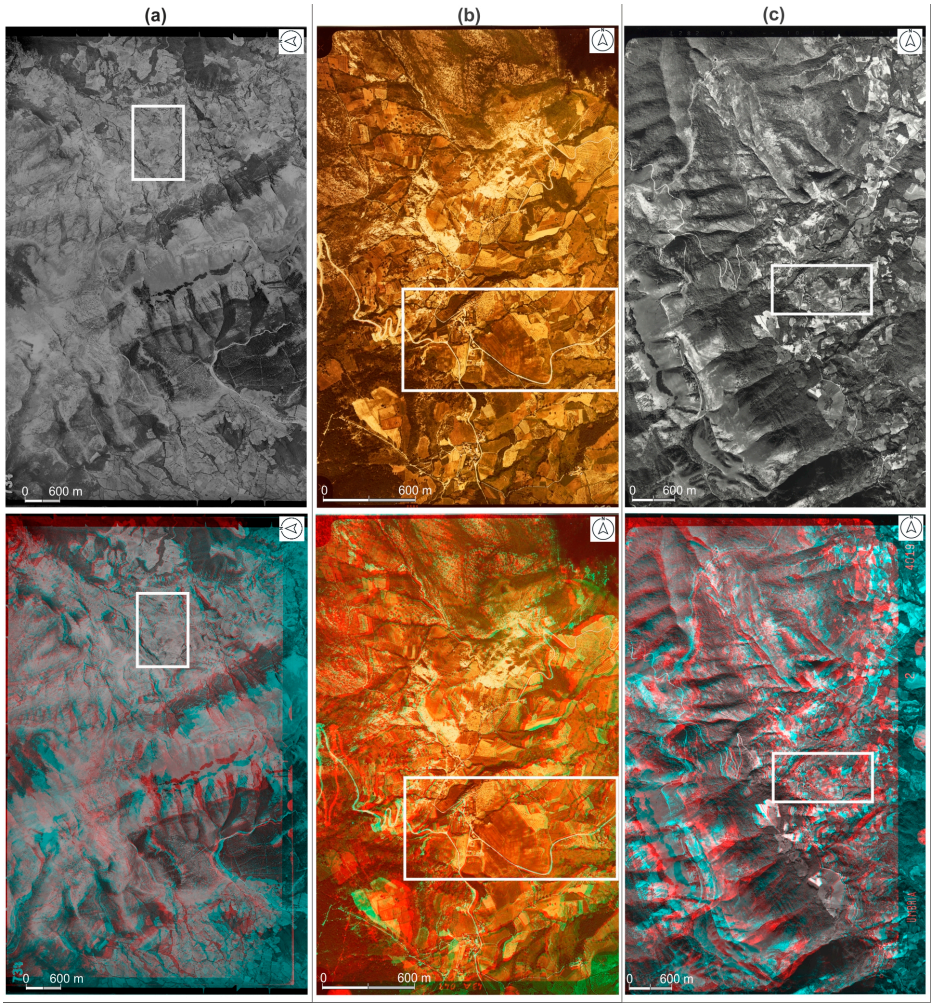

Figure 5. Multitemporal photo aerial images with anaglyphs generated with StereoPhoto Maker software (3D glasses for proper viewing are required). (**a**) AR 06–"Volo GAI" B/W 1954 photogram 734 with the anaglyph beneath built with flights 734–735; (**b**) "Volo Umbria a colori" photogram 43A–50 with the anaglyph beneath built with flights A43–49 and A43–50; (**c**) "Volo AR34" B/W 1997 photogram 2-4020 with the anaglyph beneath built with flights 2-4019 and 2-4020. The white boxes indicate the study area.

Because the data from the in situ conventional displacements monitoring system date back more than 20 years [35], updated information about ground deformations was extracted from PSInSAR analysis. Buildings are sensitive to movements caused by ground

deformation, so the temporal distribution of deformations of PS allows for understanding the landslide evolution, even in periods before the direct monitoring in the field.

Figures 6 and 7 show the cumulative displacements extracted from different selected PS. In the new urban area of the Montemartano village—extensively affected by building and dwelling damage (Figure 2—the analysis of ground deformations with ERS and ENVISAT satellite (ascending) cannot be carried out due to the absence of measurement points (Figure 6a). On the contrary, several PS represent the CSK ascending dataset well (Figure 6b–d). PS clearly show a period with no or slow ground deformations (until October 2012), followed by significant movements that have persisted up to the end of the time series (velocity ranging from −10 to about −15 mm/y). The same behavior is observed by analyzing the CSK descending dataset (Figure 7b), with a ground deformation velocity of 10 mm/year detected starting at the beginning of autumn 2012.

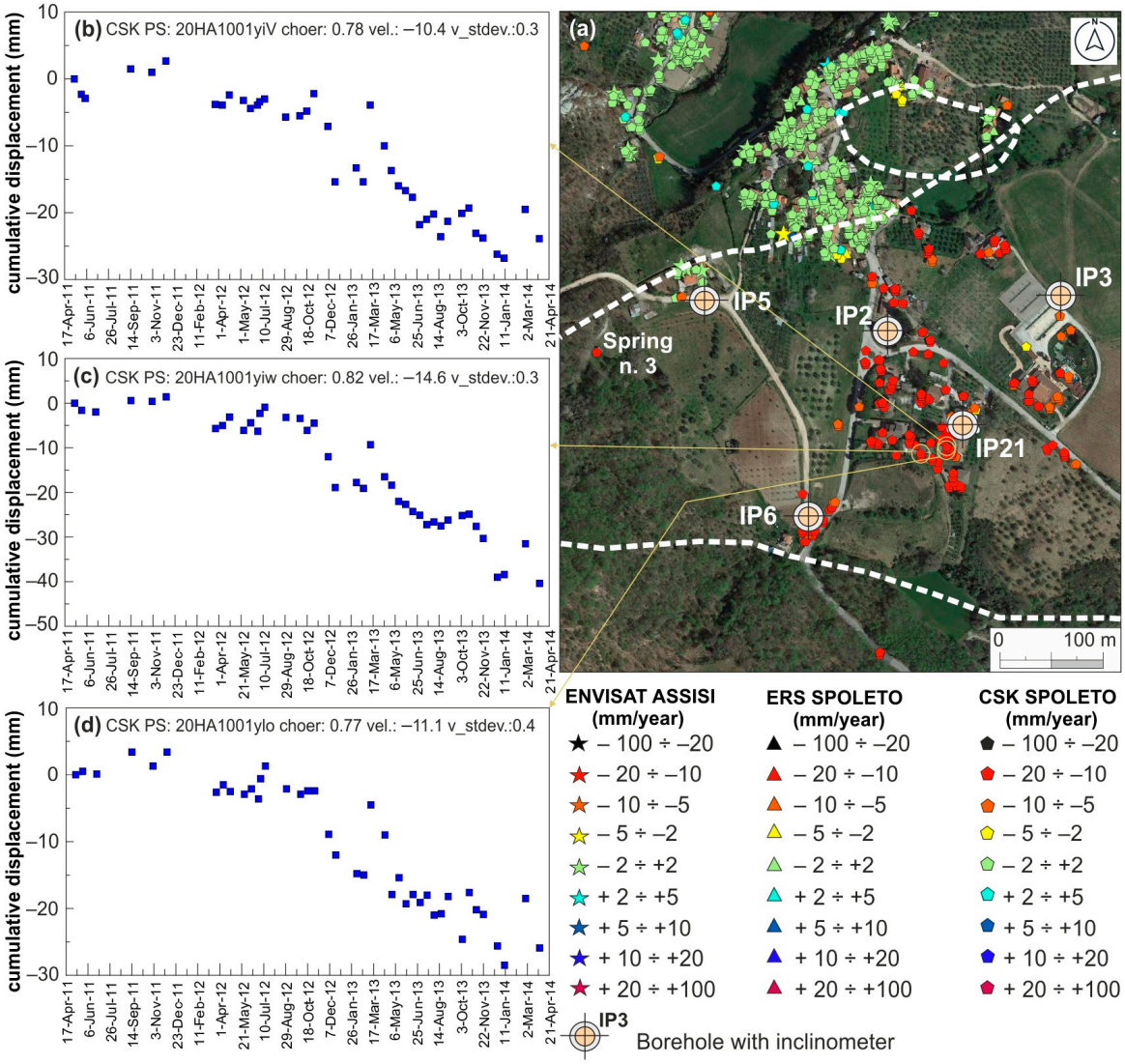

Figure 6. Cumulative displacement extracted from three PS points (only CSK ascending dataset have been selected). Data are in Table S1. (**a**) Location of PS; (**b**) cumulative displacement of CSK PS: 20HA1001yiV; (**c**) cumulative displacement of CSK PS: 20HA1001yiw; (**d**) cumulative displacement of CSK PS 20HA1001ylo. Data are in Table S1.

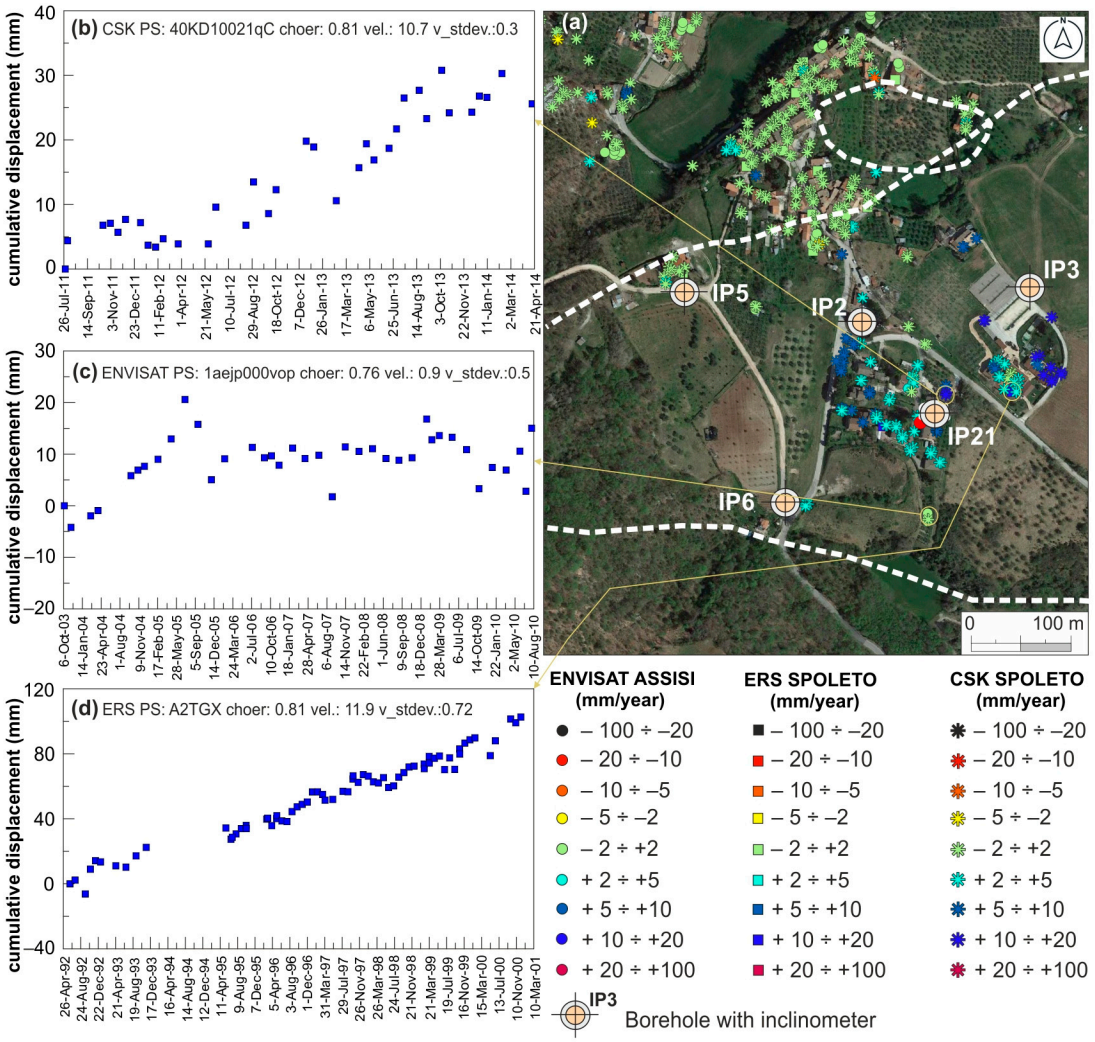

Figure 7. Cumulative displacement extracted from three PS points. (**a**) Location of PS; (**b**) cumulative displacement of CSK PS: 40KD10021qC; (**c**) cumulative displacement of ENVISAT PS: 1aejp000vop; (**d**) cumulative displacement of ERS PS: A2TGX. Data are in Table S1.

Using the ERS and ENVISAT datasets allows the monitoring of the landslide in two other periods, April 1992–December 2000 and October 2003–August 2010, respectively (Figure 7c,d). The ERS descending dataset, apart from the data gap between 1993 and 1995, recorded a continuous ground deformation with a velocity of about 12 mm/year (Figure 7d). On the contrary, the ENVISAT descending dataset (Figure 7c) shows very low velocities with periods characterized by constant cumulative displacement values around 10 mm (September 2005–September 2008).

Figure 8 compares of the landslide polygon perimeter obtained in the present study with those reported by [33] and by the official landslide inventory (Piano di Assetto Idrogeologico, PAI). In the historic center of Montemartano, the data extracted from the PSInSAR, in all the datasets, reveal no significant displacements (rate of velocity range between −2.0 and 2.0 mm/year), indicating that this zone can be considered stable. Overall, the landslide polygon perimeter presented here (area of about 520,000 m^2) matches that of [33], except in the head scarp area where the spring draining tunnels are located. The PS available for the CSK ascending dataset close to the spring n. 3 intake work (Figure 6) showed a velocity of the landslide mass of −10 ÷ −20 mm/year in the 2011–2014 period, confirming the displacement of the debris body outcropping along the slope (see Section 2.1). Considering the depths of the slip recorded by inclinometers (Figure 3) and the landslide area, the landslide volume is estimated in about 7.7 Mm^3.

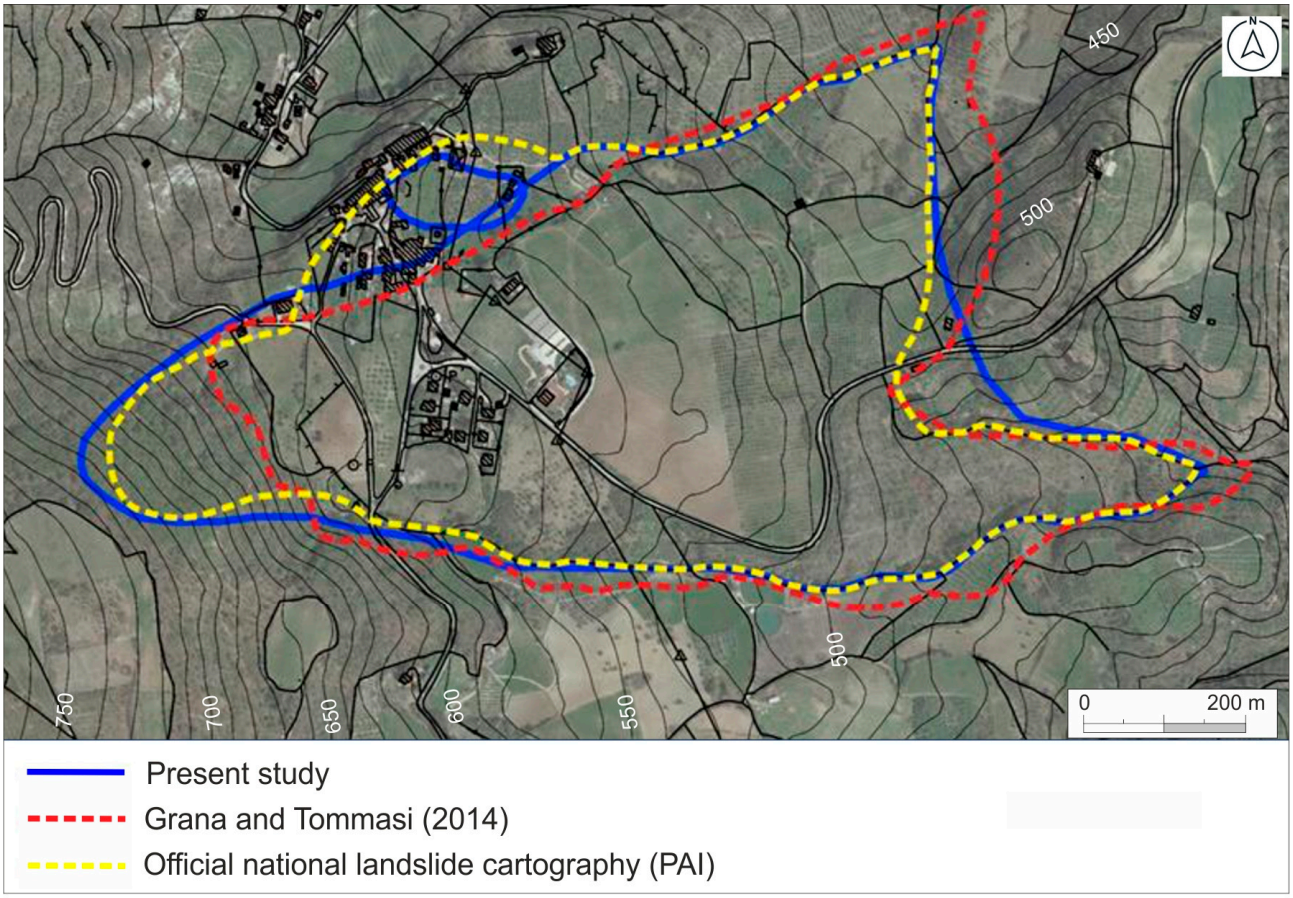

Figure 8. Comparison of the landslide polygon perimeter obtained in the present study with those reported by [33] and by the official national landslide cartography (Piano di Assetto Idrogeologico, PAI).

The application of the procedure for hazard and risk assessment proposed by PAI (Figure 4) allowed us to present a revision of the hazard and risk levels for the Montemartano landslide. Step by step the procedure followed:

- Step 1: Total landslide volume of about 7.7 Mm^3 with very-high intensity (4);
- Step 2: Very-high frequency (more than three events over 50 years), corresponding to a hazard level 44 (P4);
- Step 3: Thirty-four buildings and streets on which a structural damage can occur (300);
- Step 4: By combining the hazard (44) and the structural damage (300), a specific risk of 344 is obtained, falling in the risk level R4 (Step 5).

Compared to the current PAI planning, the total risk of the landslide area is re-classified from R3 to R4, not including some buildings in the historic center of Montemartano (Figure 8).

5. Discussion

The case presented provides useful insight into the use of the PSInSAR technique in revising landslide mapping. Among the satellites used, the data coverage of CSK in the new urban area of Montemartano is higher than ERS and ENVISAT satellites, also allowing the quantification of the deformation history in periods with no monitoring in the field. The cumulated displacements recorded in 2011–2014 (CSK) and 2003–2005 (ENVISAT) can be discussed considering the meteo-climatic conditions at that period (Figure 9a,b). As shown by both CSK ascending and descending datasets (Figure 9a), long periods characterized by average movements of about 12 mm/year were detected in the new urban area of Montemartano village, preceded by several months with very low or no movements (e.g., during April 2011–September 2012 period). Similar results were obtained

in another observation period (2003–2005) by using the ENVISAT descending dataset (Figure 9b). As reported by Wasowski and Pisano [47], data from sparse inclinometer and more spatially continuous remote sensing measurements coupled with rainfall records can provide information on the temporal variability of landslide motions. The sudden increase in displacements observed in the two datasets correlates with an increase in precipitation after prolonged dry periods. In Central Italy, and generally in the Mediterranean Region, the 2001–2003 and 2011–2012 periods were characterized by low-rain periods [48–50], followed by prolonged rainfall periods, with positive anomaly from mean monthly rainfall, having significant effects on the landslide movement. Although interactions between ongoing climate change and landslide behavior are challenging to assess [51], the shift from drought to extreme rainfalls has recently been identified as responsible for driving the re-activation of landslides [52]. According to Zheng et al. [53], droughts induce the cracking of clayey soils, degrading the hydraulic–mechanical properties. The evolution of the crack network significantly changes the pore distribution of soils and the seepage paths for fluids [54,55], allowing the infiltration of water and increasing the pore pressure in the landslide body during wet periods.

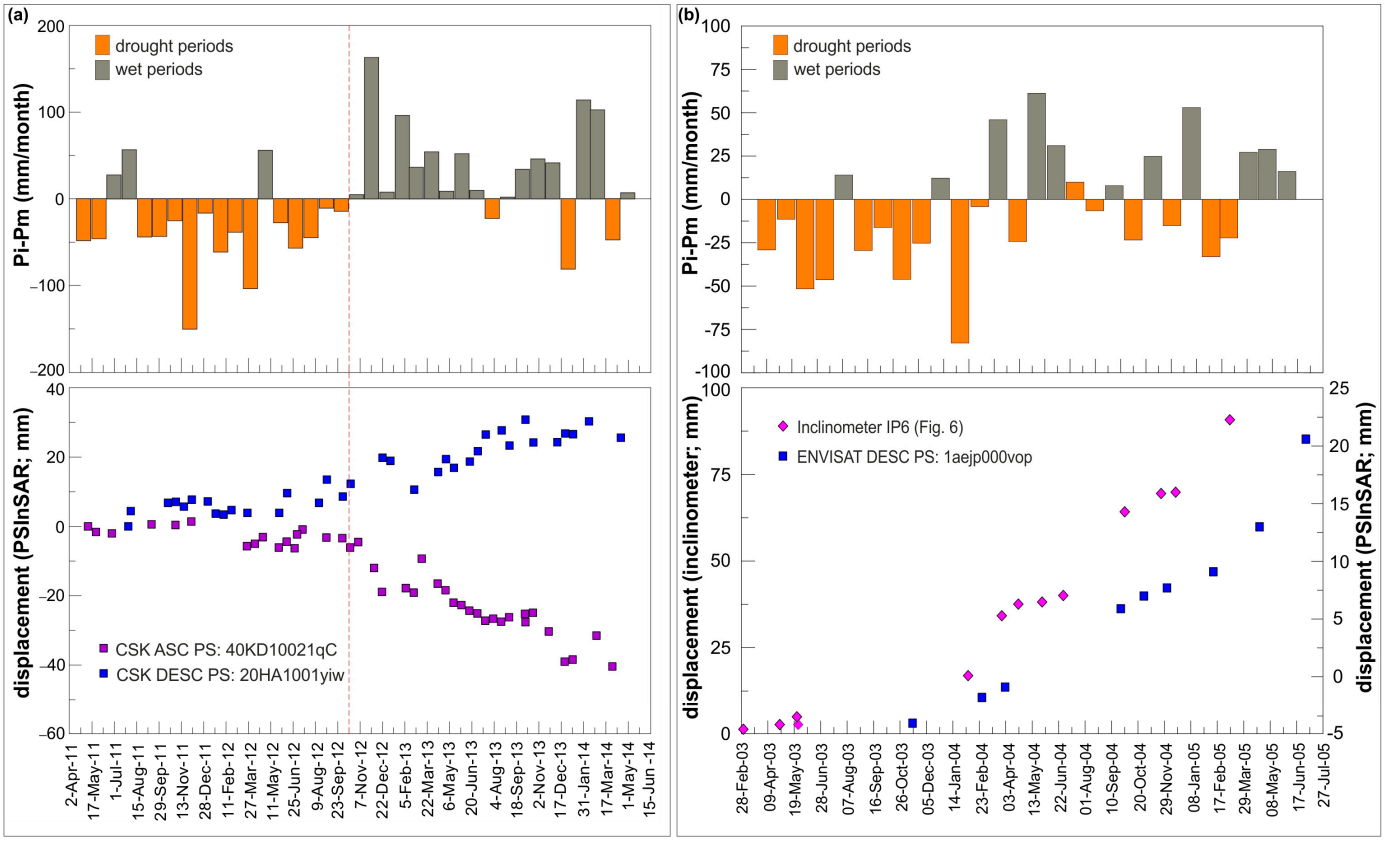

Figure 9. (**a**) Cumulative displacement of two CSK PS points (Figures 5c and 6b) vs. rainfall anomaly from mean monthly rainfall (Montemartano rain gauge data); (**b**) Cumulative displacement of the ENVISAT PS point in Figure 6c and displacement registered at inclinometer IP6 vs. rainfall anomaly from mean monthly rainfall (San Silvestro rain gauge data). Pi = rainfall of month i; Pm = mean rainfall of month i.

Figure 9b also shows a comparative analysis between PS displacements (ENVISAT) and those recorded at inclinometer IP6, located about 100 m west of the PS investigated. The two monitoring techniques are consistent in terms of cumulative deformation trend, and—as expected—the PS recorded lower deformation than the inclinometer. The comparison confirms that the in situ measurements agree with the PSInSAR; thus, landslide mass displacements can be estimated using either set of measurements. Moreover, the findings

of PSInSAR data in periods with no on-site monitoring (e.g., after 2005), can be used to improve the monitoring system's design.

6. Conclusions

The satellite and ground-based displacement data analysis on a complex landslide in Central Italy has shown a good agreement between PS displacement rates and the in situ measurements. Moreover, the PSInSAR technique gave additional information to be integrated with that derived from conventional methods for landslide mapping. The landslide polygon has been re-examined thanks to the PSInSAR technique. All the available datasets (ERS, ENVISAT, and CSK) provided a high density of stable PS over the Montemartano historic center; therefore, some buildings have actually been removed from the PAI polygon.

Although this type of landslide is characterized by slow movements and a complex pattern of displacements, the transition between prolonged droughts and wet periods played an essential role in driving the re-activation of the landslide. Identifying the behavior of the landslide to rainfall conditions offers an important insight into the velocities and cumulative displacements to be expected during similar stages of enhanced landslide activity.

The findings can be helpful to support urban planners in implementing efficient mitigation techniques to reduce landslide damage.

Supplementary Materials: Surface displacement values can be downloaded at https://www.mdpi.com/article/10.3390/rs15051221/s1, Table S1: Displacement values of PS of ENVISAT, CSK, and ERS datasets.

Author Contributions: Conceptualization, L.D.M. and C.C.; methodology, L.D.M., R.C., V.C., F.G., G.P., C.R. and C.C.; software, V.C., F.G., G.P. and C.R.; validation, L.D.M., R.C., V.C., F.G., G.P., C.R. and C.C.; formal analysis, L.D.M., R.C., V.C., F.G., G.P., C.R., B.M.S. and C.C.; investigation, L.D.M., R.C., V.C., F.G., G.P., C.R., B.M.S. and C.C.; resources, C.C.; data curation, L.D.M., V.C., F.G., G.P., C.R. and C.C.; writing—original draft preparation, L.D.M., R.C., V.C., F.G., G.P., C.R., B.M.S. and C.C.; writing—review and editing, L.D.M., R.C., V.C., F.G., G.P., C.R., B.M.S. and C.C.; visualization, L.D.M., R.C., V.C., F.G., G.P. and C.R.; supervision, L.D.M. and C.C.; project administration, L.D.M. and C.C.; funding acquisition, C.C. All authors have read and agreed to the published version of the manuscript.

Funding: This research was funded by Autorità di Bacino Distrettuale dell'Appennino Centrale, ABDAC (funding n. ABDACCENCETTI21) in the framework of the research agreement with *ABDAC and Struttura Commissariale Ricostruzione Sisma 2016*. Title of the project: "*Revisione degli areali a pericolosità da frana elevata P3 e molto elevata P4 delle aree PAI interagenti con le previsioni di ricostruzione nei Comuni interessati dagli eventi sismici verificatisi a far data dal 24 agosto 2016–2017*" (Revision of P3 and P4 hazard areas of landslides interfering with the reconstruction predictions in municipalities affecting by the 2016–2017 seismic sequence in Central Italy).

Data Availability Statement: Publicly available datasets were analyzed in this study. These data can be found here: http://www.pcn.minambiente.it/mattm/servizio-distribuzione-dati-pst/, accessed on 9 January 2023.

Acknowledgments: The authors wish to thank ABDAC and Struttura Commissariale per la ricostruzione Sisma 2016 for providing the resources to carry out the research.

Conflicts of Interest: The authors declare no conflict of interest.

References

1. Van Den Eeckhaut, M.; Hervás, J. State of the art of national landslide databases in Europe and their potential for assessing landslide susceptibility, hazard and risk. *Geomorphology* **2012**, *139–140*, 545–558. [CrossRef]
2. Alexander, D.E. A brief survey of GIS in mass-movement studies, with reflections on theory and methods. *Geomorphology* **2008**, *94*, 261–267. [CrossRef]
3. Assilzadeh, H.; Levy, J.K.; Wang, X. Landslide Catastrophes and Disaster Risk Reduction: A GIS Framework for Landslide Prevention and Management. *Remote Sens.* **2010**, *2*, 2259–2273. [CrossRef]

4. Zhong, C.; Liu, Y.; Gao, P.; Chen, W.; Li, H.; Hou, Y.; Nuremanguli, T.; Ma, H. Landslide mapping with remote sensing: Challenges and opportunities. *Remote Sens.* **2020**, *41*, 1555–1581. [CrossRef]
5. Guzzetti, F.; Mondini, A.C.; Cardinali, M.; Fiorucci, F.; Santangelo, M.; Chang, K.T. Landslide inventory maps: New tools for an old problem. *Earth-Sci. Rev.* **2012**, *112*, 42–66. [CrossRef]
6. Bardi, F.; Frodella, W.; Ciampalini, A.; Bianchini, S.; Del Ventisette, C.; Gigli, G.; Fanti, R.; Moretti, S.; Basile, G.; Casagli, N. Integration between ground based and satellite SAR data in landslide mapping: The San Fratello case study. *Geomorphology* **2014**, *223*, 45–60. [CrossRef]
7. Cencetti, C.; Conversini, P.; Radicioni, F.; Ribaldi, C.; Selli, S.; Tacconi, P. The Evolution of Montebestia Landslide (Umbria, Central Italy). Site Investigations, In-Situ Tests and GPS Monitoring. *Phys. Chem. Earth (B)* **2000**, *25*, 799–808. [CrossRef]
8. Meisina, C.; Zucca, F.; Notti, D.; Colombo, A.; Cucchi, A.; Savio, G.; Gannico, C.; Bianchi, M. Geological interpretation of PSInSAR data at regional scale. *Sensors* **2008**, *8*, 7469–7492. [CrossRef]
9. Calò, F.; Calcaterra, D.; Iodice, A.; Parise, M.; Ramondini, M. Assessing the activity of a large landslide in southern Italy by ground-monitoring and SAR interferometric techniques. *Int. J. Remote Sens.* **2012**, *33*, 3512–3530. [CrossRef]
10. Allasia, P.; Manconi, A.; Giordan, D.; Baldo, M.; Lollino, G. ADVICE: A New Approach for Near-Real-Time Monitoring of Surface Displacements in Landslide Hazard Scenarios. *Sensors* **2013**, *13*, 8285–8302. [CrossRef] [PubMed]
11. Rosi, A.; Vannocci, P.; Tofani, V.; Gigli, G.; Casagli, N. Landslide Characterization Using Satellite Interferometry (PSI), Geotechnical Investigations and Numerical Modelling: The Case Study of Ricasoli Village (Italy). *Int. J. Geosci.* **2013**, *4*, 904–918. [CrossRef]
12. Scaioni, M.; Longoni, L.; Melillo, V.; Papini, M. Remote Sensing for Landslide Investigations: An Overview of Recent Achievements and Perspectives. *Remote Sens.* **2014**, *6*, 9600–9652. [CrossRef]
13. Taramelli, A.; Di Matteo, L.; Ciavola, P.; Guadagnano, F.; Tolomei, C. Temporal evolution of patterns and processes related to subsidence of the coastal area surrounding the Bevano River mouth (Northern Adriatic)—Italy. *Ocean Coast. Manag.* **2015**, *108*, 74–88. [CrossRef]
14. Mazzanti, P.; Bozzano, F.; Cipriani, I.; Prestininzi, A. New insights into the temporal prediction of landslides by a terrestrial SAR interferometry monitoring case study. *Landslides* **2015**, *12*, 55–68. [CrossRef]
15. Di Matteo, L.; Romeo, S.; Kieffer, D.S. Rock fall analysis in an Alpine area by using a reliable integrated monitoring system: Results from the Ingelsberg slope (Salzburg Land, Austria). *Bull. Eng. Geol. Environ.* **2017**, *76*, 413–420. [CrossRef]
16. Romeo, S.; Di Matteo, L.; Kieffer, D.S.; Tosi, G.; Stoppini, A.; Radicioni, F. The Use of Gigapixel Photogrammetry for the Understanding of Landslide Processes in Alpine Terrain. *Geosciences* **2019**, *9*, 99. [CrossRef]
17. Miele, P.; Di Napoli, M.; Novellino, A.; Calcaterra, D.; Mallorqui, J.J.; Di Martire, D. SAR data and field surveys combination to update rainfall-induced shallow landslide inventory. *Remote Sens. Appl. Soc. Environ.* **2022**, *26*, 100755. [CrossRef]
18. Trigila, A.; Iadanza, C.; Bussettini, M.; Lastoria, B. *Dissesto Idrogeologico in Italia: Pericolosità e Indicatori di Rischio*; Ispra, Italy, 2018; Rapporti 287/2018; 159p. Available online: https://www.isprambiente.gov.it/it/pubblicazioni/rapporti/dissesto-idrogeologico-in-italia-pericolosita-e-indicatori-di-rischio-edizione-2021 (accessed on 9 January 2023).
19. Petitta, M.; Mastrorillo, L.; Preziosi, E.; Banzato, F.; Barberio, M.D.; Billi, A.; Cambi, C.; De Luca, G.; Di Carlo, G.; Di Curzio, D.; et al. Water table and discharge changes associated with the 2016–2017 seismic sequence in central Italy: Hydrogeological data and a conceptual model for fractured carbonate aquifers. *Hydrogeol. J.* **2018**, *26*, 1009–1026. [CrossRef]
20. Valerio, E.; Tizzani, P.; Carminati, E.; Doglioni, C.; Pepe, S.; Petricca, P.; De Luca, C.; Bignami, C.; Solaro, G.; Castaldo, R.; et al. Ground Deformation and Source Geometry of the 30 October 2016 Mw 6.5 Norcia Earthquake (Central Italy) Investigated Through Seismological Data, DInSAR Measurements, and Numerical Modelling. *Remote Sens.* **2018**, *10*, 1901. [CrossRef]
21. Valigi, D.; Mastrorillo, L.; Cambi, C.; Barchi, M.R.; Cardellini, C.; Checcucci, R.; Di Matteo, L.; Frondini, F.; Mirabella, F.; Viaroli, S.; et al. Springs discharge variations induced by strong earthquakes: The Mw 6.5 Norcia event (Italy, October 30th 2016). *Rend. Online Soc. Geol. Ital.* **2019**, *47*, 141–146. [CrossRef]
22. Di Matteo, L.; Dragoni, W.; Azzaro, S.; Pauselli, C.; Porreca, M.; Bellina, G.; Cardaci, W. Effects of earthquakes on the discharge of groundwater systems: The case of the 2016 seismic sequence in the Central Apennines, Italy. *J. Hydrol.* **2020**, *583*, 124509. [CrossRef]
23. Fronzi, D.; Di Curzio, D.; Rusi, S.; Valigi, D.; Tazioli, A. Comparison between Periodic Tracer Tests and Time-Series Analysis to Assess Mid-and Long-Term Recharge Model Changes Due to Multiple Strong Seismic Events in Carbonate Aquifers. *Water* **2020**, *12*, 3073. [CrossRef]
24. Di Matteo, L.; Capoccioni, A.; Porreca, M.; Pauselli, C. Groundwater-Surface Water Interaction in the Nera River Basin (Central Italy): New Insights after the 2016 Seismic Sequence. *Hydrology* **2021**, *8*, 97. [CrossRef]
25. Cambi, C.; Mirabella, F.; Petitta, M.; Banzato, F.; Beddini, G.; Cardellini, C.; Fronzi, D.; Mastrorillo, L.; Tazioli, A.; Valigi, D. Reaction of the carbonate Sibillini Mountains Basal aquifer (Central Italy) to the extensional 2016–2017 seismic sequence. *Sci. Rep.* **2022**, *12*, 22428. [CrossRef]
26. Romeo, S.; Di Matteo, L.; Melelli, L.; Cencetti, C.; Dragoni, W.; Fredduzzi, A. Seismic-induced rockfalls and landslide dam following the October 30, 2016 earthquake in Central Italy. *Landslides* **2017**, *14*, 1457–1465. [CrossRef]
27. Caprari, P.; Della Seta, M.; Martino, S.; Fantini, A.; Fiorucci, M.; Priore, T. Upgrade of the CEDIT database of earthquake-induced ground effects in Italy. *Ital. J. Eng. Geol. Environ.* **2018**, *2*, 23–39. [CrossRef]

28. Martino, S.; Bozzano, F.; Caporossi, P.; D'angiò, D.; Della Seta, M.; Esposito, C.; Fantini, M.; Fiorucci, L.; Giannini, L.M.; Iannucci, R.; et al. Impact of landslides on transportation routes during the 2016–2017 Central Italy seismic sequence. *Landslides* **2019**, *16*, 1221–1241. [CrossRef]
29. Farabollini, P.; De Pari, P.; Discenza, M.E.; Minnillo, M.; Carabella, C.; Paglia, G.; Miccadei, E. Geomorphological evidence of debris flows and landslides in the Pescara del Tronto area (Sibillini Mts, Marche Region, Central Italy). *J. Maps* **2021**, *17*, 90–99. [CrossRef]
30. Cencetti, C.; Di Matteo, L. Mitigation measures preventing floods from landslide dams: Analysis of pre-and post-hydrologic conditions upstream a seismic-induced landslide dam in Central Italy. *Environ. Earth Sci.* **2022**, *81*, 403. [CrossRef]
31. Santangelo, M.; Marchesini, I.; Bucci, F.; Cardinali, M.; Cavalli, M.; Crema, S.; Marchi, L.; Alvioli, M.; Guzzetti, F. Exposure to landslides in rural areas in Central Italy. *J. Maps* **2021**, *17*, 124–132. [CrossRef]
32. Ferretti, A.; Prati, C.; Rocca, F. Permanent Scatterers in SAR Interferometry. *IEEE Trans. Geosci. Remote Sens.* **2001**, *39*, 8–20. [CrossRef]
33. Grana, V.; Tommasi, P. A deep-seated slow movement controlled by structural setting in marly formations of Central Italy. *Landslides* **2014**, *11*, 195–212. [CrossRef]
34. Barchi, M. Una Sezione Geologica Bilanciata Attraverso il Settore Meridionale Dell'Appennino Umbro-Marchigiano: L'Acquasparta-Spoleto-Accumoli. *Studi Geol. Camerti* **1991**, *1*, 347–362. Available online: http://193.204.8.201:8080/jspui/bitstream/1336/579/1/Vol.%20Speciale%201991-1%20Capitolo%2036.pdf (accessed on 14 January 2023).
35. Alta Scuola. Studio del Fenomeno Franoso Interessante l'Area Posta a sud del Nucleo Storico dell'Abitato di Montemartano. Unpublished Technical Report; Comune di Spoleto, Italy, 2017; 135p. Available online: https://drive.google.com/file/d/1OL4XgIl2QlkSPf9i_VWvF1hFryV1KrDC/view?usp=share_link (accessed on 14 January 2023).
36. Regione Umbria. Comune di Spoleto. Area a rischio di frana in località Montemartano. Report monitoraggio inclinometro S21 e analisi dati interferometrici satellitari. Unpublished Technical report; Regione Umbria, Italy, 2019; 3p. Available online: https://drive.google.com/file/d/1npyaEgimxGWqN_NApUnE4rNuivCG6NAn/view?usp=share_link (accessed on 14 January 2023).
37. Verstappen, H.T. Photointerpretation. In *General Geology. Encyclopedia of Earth Science*; Springer: Boston, MA, USA, 1988. [CrossRef]
38. Zanutta, A.; Baldi, P.; Bitelli, G.; Cardinali, M. Qualitative and quantitative photogrammetric techniques for multi-temporal landslide analysis. *Ann. Geophisics* **2006**, *49*, 1067–1080. Available online: https://www.earth-prints.org/bitstream/2122/2124/1/14.pdf (accessed on 13 January 2023). [CrossRef]
39. Cencetti, C.; Di Matteo, L.; Romeo, S. Analysis of Costantino landslide dam evolution (Southern Italy) by means of satellite images, aerial photos, and climate data. *Geosciences* **2017**, *7*, 30. [CrossRef]
40. Cruden, D.M.; Varnes, D.J. Landslide Types and Processes. *Transp. Res. Board* **1996**, *247*, 36–75.
41. Bürgmann, R.; Rosen, P.A.; Fielding, E.J. Synthetic aperture radar interferometry to measure Earth's surface topography and its deformation. *Annu. Rev. Earth Planet. Sci.* **2000**, *28*, 169–209. [CrossRef]
42. Colombo, A.; Mallen, L.; Pispico, R.; Giannico, C.; Bianchi, M.; Savio, G. Mappatura Regionale Delle Aree Monitorabili Mediante l'uso Della Tecnica PS. In Proceedings of the 10° Conferenza Nazionale ASITA, Bolzano, Italy, November 2006. Available online: https://site.tre-altamira.com/wp-content/uploads/2006_Mappatura_regionale_delle_aree_monitorabili_mediante_uso_della_Tecnica_PS.pdf (accessed on 14 December 2022).
43. Bottero, D.; Poggi, F.; Cespa, S. Nuove tecnologie di analisi delle frane: Il monitoraggio satellitare. *Quarry Constr.* **2006**, 87–97. Available online: https://site.tre-altamira.com/wp-content/uploads/2006_Il_monitoraggio_satellitare_Primi_risultati_in_Liguria_della_sperimentazione_utilizzo_della_Tecnica_PSInSAR.pdf (accessed on 14 December 2022).
44. Pigorini, A.; Ricci, M.; Sciotti, A.; Giannico, C.; Tamburini, A. La Tecnica PSInSAR di Telerilevamento Satellitare Applicata al Progetto ed alla Realizzazione delle Infrastrutture Ferroviarie. *Ing. Ferrov.* **2010**, *IX*, 729–757. Available online: https://site.tre-altamira.com/wp-content/uploads/2010_Satellite_remote-sensing_PSInSAR_technique_applied_to_design_and_construction_of_railway_infrastructures.pdf (accessed on 14 December 2022).
45. Ciampalini, A.; Bardi, F.; Bianchini, S.; Frodella, W.; Del Ventisette, C.; Moretti, S.; Casagli, N. Analysis of building deformation in landslide area using multisensor PSInSAR™ technique. *Int. J. Appl. Earth Obs. Geoinf.* **2014**, *33*, 166–180. [CrossRef] [PubMed]
46. PAI. Piano Stralcio di Assetto Idrogeologico. Autorità di Bacino del Fiume Tevere. Delibera N. 114. 5 April 2006. (In Italian). Available online: https://www.abtevere.it/sites/default/files/datisito/relazione_generale_pai.pdf (accessed on 10 February 2023).
47. Wasowski, J.; Pisano, L. Long-term InSAR, borehole inclinometer, and rainfall records provide insight into the mechanism and activity patterns of an extremely slow urbanized landslide. *Landslides* **2020**, *17*, 445–457. [CrossRef]
48. Di Matteo, L.; Valigi, D.; Cambi, C. Climatic characterization and response of water resources to climate change in limestone areas: Considerations on the importance of geological setting. *J. Hydrol. Eng.* **2013**, *18*, 773–779. [CrossRef]
49. Raymond, F.; Ullmann, A.; Camberlin, P.; Drobinski, P.; Smith, C.C. Extreme dry spell detection and climatology over the Mediterranean Basin during the wet season. *Geophys. Res. Lett.* **2016**, *43*, 7196–7204. [CrossRef]
50. Di Matteo, L.; Dragoni, W.; Maccari, D.; Piacentini, S.M. Climate change, water supply and environmental problems of headwaters: The paradigmatic case of the Tiber, Savio and Marecchia rivers (Central Italy). *Sci. Total Environ.* **2017**, *598*, 733–748. [CrossRef] [PubMed]
51. Gariano, S.L.; Guzzetti, F. Landslides in a changing climate. *Earth-Sci. Rev.* **2016**, *162*, 227–252. [CrossRef]

52. Handwerger, A.L.; Huang, M.H.; Fielding, E.J.; Booth, A.M.; Bürgmann, R. A shift from drought to extreme rainfall drives a stable landslide to catastrophic failure. *Sci. Rep.* **2019**, *9*, 1569. [CrossRef]
53. Zeng, H.; Tang, C.-S.; Cheng, Q.; Zhu, C.; Yin, L.-Y.; Shi, B. Drought-induced soil desiccation cracking behavior with consideration of basal friction and layer thickness. *Water Resour. Res.* **2020**, *56*, e2019WR02694. [CrossRef]
54. Stewart, R.D. A dynamic multidomain Green-Ampt infiltration model. *Water Resour. Res.* **2018**, *54*, 6844–6859. [CrossRef]
55. Yoshida, S.; Hallett, P.D. Impact of hydraulic suction history on crack growth mechanics in soil. *Water Resour. Res.* **2008**, *44*, W00C01. [CrossRef]